

# Quarterly Report

**Date of report:** June 26, 2007

**For quarter ending:** June 30, 2007

**Agreement number:** DTPH56-06-X-000029

**Agreement Time period:** June 30, 2006 to June 29, 2008

**Project:** Mechanical Properties and Crack Behavior in Line Pipe Steels

**Prepared by:** NIST, Materials Reliability Division

## **Project Tasks:**

**Task 1:** Fatigue crack growth

**Task 2:** Hydrogen charged fatigue crack growth

**Task 3:** CTOA testing and modeling

**Task 4:** Fracture surface examination

**Task 5:** Method for determination of yield strength in high strength pipeline steels and welds

**Task 6:** Other tasks as assigned

**Task 7:** Reporting

NIST-Boulder received the contract for this program in early June 2006. Our efforts are focused on CTOA testing of pipeline steels, weldments and heat affected zones (girth and seam), and the development of a model for our dynamic ductile fracture experiments. Last quarter we completed the design and implementation of the "high-speed" test machine, and this quarter we have improved on that version of the test system by introducing a spring loaded fixture to better simulate the actual velocity of a running crack in a pipeline. This new test set-up is expected to provide crack velocities in the range of 100 m per second or more. Full-thickness fatigue experiments are also under way and the hydrogen charged tests are coming to completion.

The following task updates should be appended to previously submitted quarterly reports.

## **Technical status of tasks:**

### **Task 1: Fatigue crack growth**

The axial fatigue tests continue at  $r=0.1$  and  $0.4$ . The axial specimen testing is almost complete and we plan to finish this portion of the effort early the next quarter. The uneven fatigue crack propagation through the pipe wall thickness in a couple of the

specimens has prompted us to investigate this phenomenon further. We have ordered software that will allow us to monitor and record the fatigue crack growth on both the ID and the OD of the pipe wall, enabling us to better understand this uneven crack growth. The software should arrive early the next quarter. Following the completion of the axial fatigue tests, we plan to start the transverse specimen fatigue testing, with the fatigue crack propagating along the pipe axis.

## **Task 2: Hydrogen charged fatigue crack growth**

To better understand the effects of hydrogen on high strength pipeline steels, we need to understand the specifics of hydrogen diffusion in the metal lattice of interest. The following section gives an overview of hydrogen diffusivity and solubility in X100. This is followed by the effect of hydrogen on fatigue properties of X100 pipeline steel.

**Hydrogen Diffusion in the Metal Lattice:** Diffusible hydrogen is transient, *i.e.* the concentration and distribution are continually changing with time. Hydrogen prefers to migrate to dislocations, second phase particles, voids, and other defects in steel. These defects influence both the distribution and the mobility of hydrogen. The “occlusive capacity” of hydrogen better describes the solubility of hydrogen in a metal lattice experiencing strain or plastic deformation such as in a pipeline, because hydrogen accumulates in these strained regions. So, the occlusive capacity is the true solubility of hydrogen in a strained condition.

The importance of the occlusive capacity of hydrogen is illustrated in Figure 1 showing how the variations in hydrogen content play a vital role on the stress state for crack growth during hydrogen assisted cracking and stress corrosion cracking. The concentration of hydrogen at a crack tip will change the mode of hydrogen cracking at a particular stress intensity factor. The curved dashed lines indicate critical combinations of stress intensity factor and hydrogen content for the cause of crack growth by the three fracture modes. The existence and position of each of the curves are microstructure dependent, so this graph does not necessarily hold true for X100 pipeline steels. Below the lowest curve, no hydrogen cracking is expected. At slightly higher hydrogen contents and increasing stress intensities, fracture modes change from intergranular to quasi-cleavage, to micro-void coalescence (for the quench and temper steel shown here).

The solubility and diffusivity of hydrogen varies greatly between iron phases. The **solubility** of hydrogen is very high for austenite and is very low for ferrite. The **diffusivity** of hydrogen is very low in austenite and very high in ferrite. Austenite acts as a diffusion barrier for hydrogen transport, while ferrite facilitates hydrogen transport. It is therefore insufficient to only measure the hydrogen content in steel. Instead, the degree of interaction of hydrogen once it enters the metal lattice is important. Permeability studies and stress-induced diffusion measurements can help explain the degree of interaction and can act as a supporting method to allow for dynamic modeling of cracking behavior.

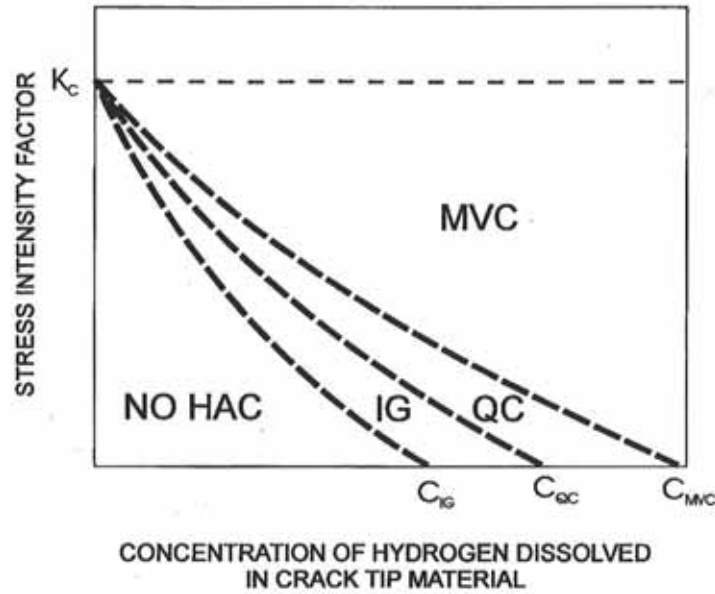
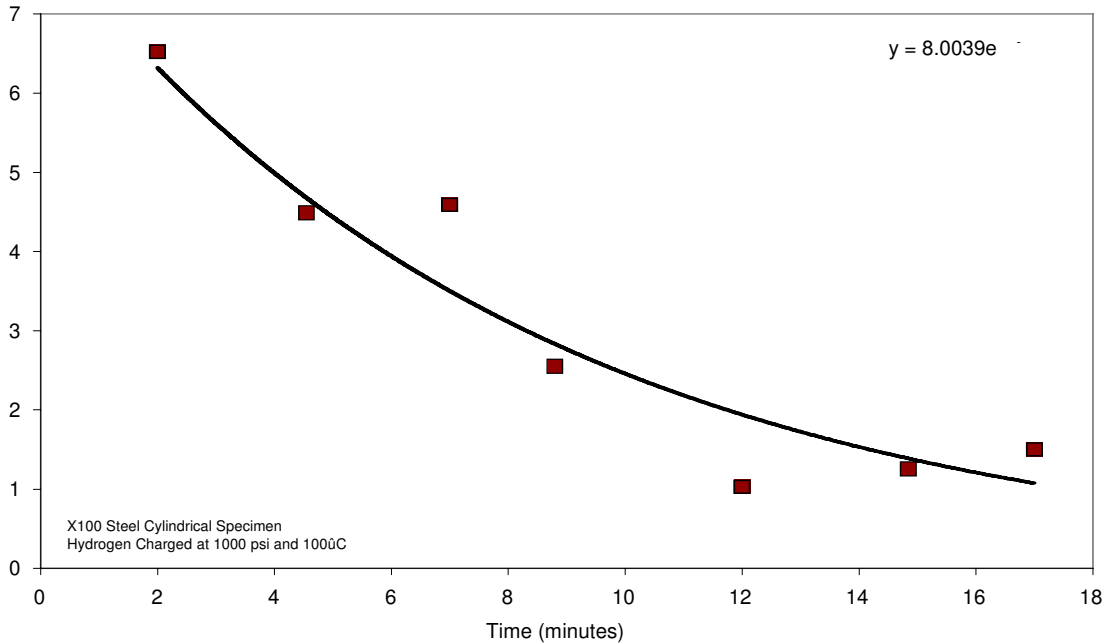


**Figure 1.** Suggested interrelationships between stress intensity factor as a function of dissolved hydrogen concentration, showing changes in hydrogen assisted cracking failure modes for a quench and temper steel (IG: Intergranular, QC: quasi-cleavage, MVC: micro-void coalescence).

**Experimental Determination of Diffusion Coefficient:** For our solubility and permeability experiments, hydrogen is introduced into the steel using a high-pressure gaseous hydrogen atmosphere. Steel pipeline specimens are hydrogen charged at a maximum pressure of 1000 psig at 100°C for specific time intervals to achieve hydrogen saturation in the specimen. Once the specimen is saturated with hydrogen, multiple techniques are used to monitor the hydrogen content as a function of time. Using Fick's 2<sup>nd</sup> Law, the diffusion coefficient can be determined from the data of hydrogen content as a function of time for the specific steel microstructure.

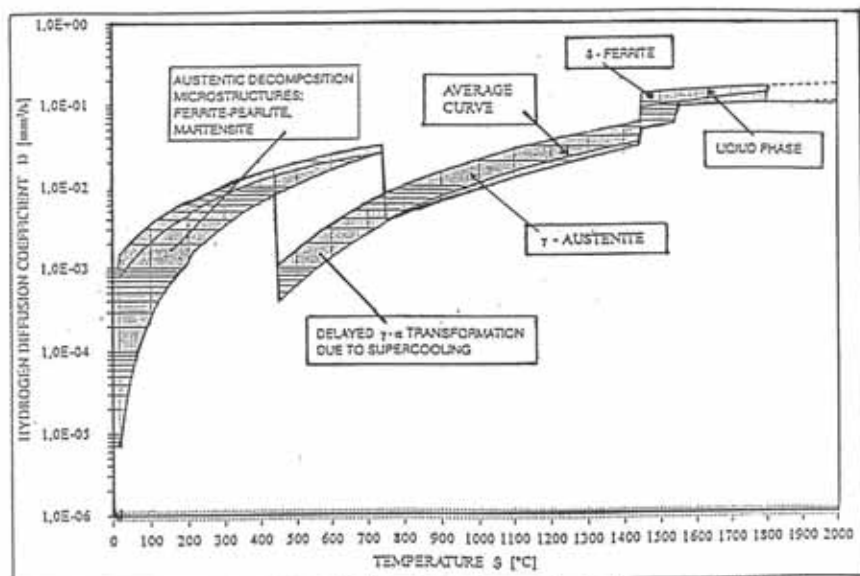
**Following** ASTM Standard G-148-97 for electrochemical diffusion coefficient measurements, hydrogen is induced on one side of specimen and we measure how long it takes for the hydrogen to reach the other side of the specimen. In the current diffusion experiments, a specimen is saturated with hydrogen and then monitored to determine the rate of hydrogen diffusion out of the specimen. The boundary conditions are the only difference between the electrochemical method in the ASTM Standard and the method currently used in this research.

Figure 2 presents experimental results where X100 pipeline steel was hydrogen charged in a gaseous atmosphere at 1000 psig and 100°C, then removed from the hydrogen atmosphere to allow the hydrogen to diffuse out of the specimen.



**Figure 2.** Hydrogen content (ppm) as a function of time for hydrogen charged X100 pipeline steel. Hydrogen content determined by gas chromatography.

The diffusion coefficient of hydrogen (at room temperature) in X100 pipeline steel has been calculated to be approximately  $4.75 \cdot 10^{-2} \text{ mm}^2/\text{sec}$ . X100 pipeline steel became saturated with hydrogen at approximately 38 ppm, but very quickly loses it due to diffusion. Figure 3 shows the diffusion coefficients as a function of temperature for various microstructures for comparison to the experimentally determined value.



**Figure 3.** Diffusion coefficient of hydrogen as a function of temperature for various microstructures.

The diffusion coefficient of hydrogen in X100 is slightly higher than the diffusion coefficients of common microstructures at room temperature. Presumably this is due to the difference in constituents in the microstructure of the X100 steel and their morphology, but this will need to be investigated further

**Influence of Hydrogen on Fatigue Crack Growth:** Fatigue tests were performed on compact tension (CT) specimens in order to evaluate the influence of the hydrogen ( $H_2$ ) during crack propagation. The test set-up is shown in Figure 4.



**Figure 4.** Fatigue experimental set-up.

The tests were performed in air. The specimens were charged for 1200 hours (50 days) at  $100^{\circ}C$  at 500 psig. The hydrogen saturation achieved through this method was approximately 39 ppm of hydrogen. In order to retain the hydrogen saturation as long as possible, the CT specimens were tinned immediately after charging and stored in liquid nitrogen until fatigue tested. The liquid nitrogen storage time was approximately 1 hour. Figure 5 presents the experimental results.

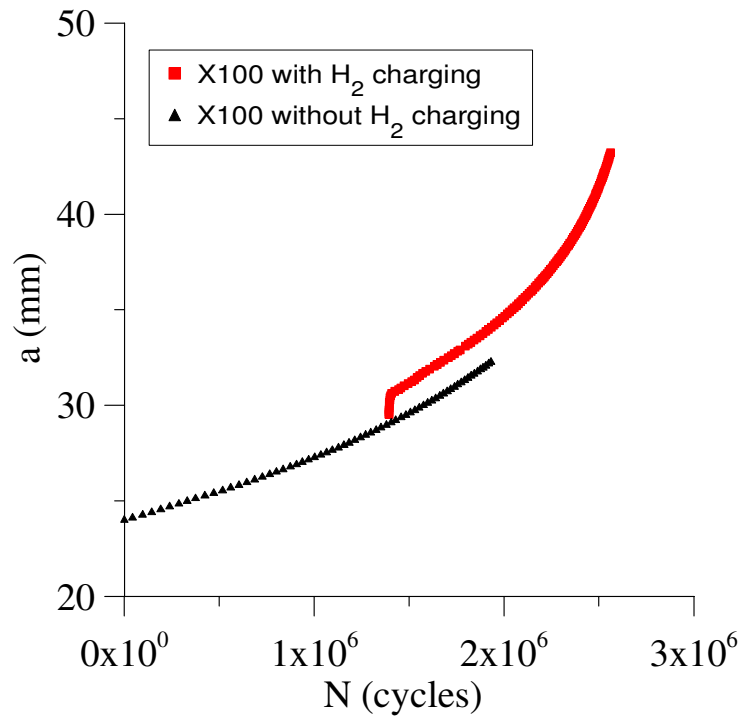
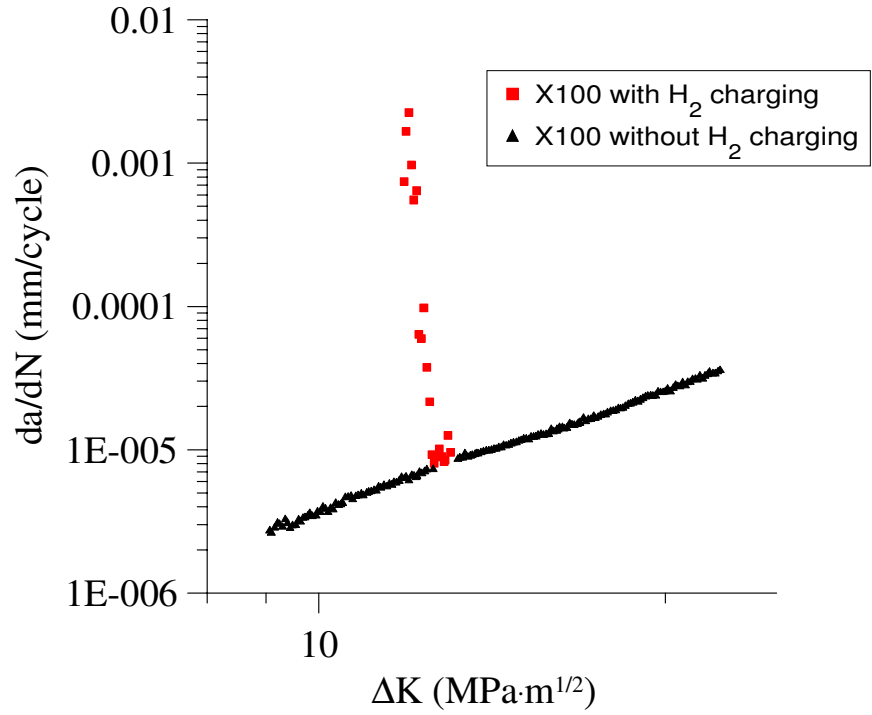


**Figure 5.** Experimental results.

The results show a very clear embrittlement effect due to hydrogen, and that the effect of the hydrogen embrittling is short for fatigue tests performed in air, due to rapid diffusion of hydrogen out of the specimen. The effect of hydrogen on  $dA/dN$  shows an increase of

more than 2 orders of magnitude! The final tests are underway now and should be complete by the end of the next quarter.

Following the completion of the testing portion of this task, we plan to conduct examinations of the fracture surfaces to determine the fracture morphology in the charged and uncharged areas.

### **Task 3: CTOA testing and modeling**

**CTOA Testing:** Quasi-static CTOA testing continues on both girth and seam weld direction fracture specimens. Previous efforts were focused on base metals with cracks oriented in the axial direction. The current effort continues to examine fracture resistance along the girth weld and girth heat affected zone (HAZ) as well as base metal in the girth direction. In addition, seam weld CTOA specimens have been machined to study ductile fracture resistance in the HAZ of the seam weld and weld metal, and specimens have been machined and tested with the crack propagating across the girth weld. Precracking of the specimens is underway and the CTOA tests should start again early in the next quarter.

**Dynamic CTOA Testing:** During this quarter, we conducted another relatively high-speed CTOA test on X65 pipeline steel using the upgraded servo-hydraulic test machine and new high-speed camera we purchased several months ago. These initial tests were set-up rather conservatively (photographing large sample areas so we did not risk missing the whole test), so they had poor resolution for CTOA measurements. However, upcoming tests will be conducted at higher resolution to provide data comparable with that gathered for our quasi-static speeds.

CTOA data is available for pipeline steels at dynamic test rates using DWTT tests, but no dynamic CTOA data is available using modified double cantilever beam specimen (MDCB). Comparison of data from these two test configurations is expected to be useful for the interpretation of CTOA data.

The crack velocity of our current high-speed tests, using the upgraded servo-hydraulic machine, is about 0.5 m per second. This is 5 orders of magnitude faster than those for our quasi-static testing, but crack growth rates during a real pipeline fracture event are even several orders of magnitude faster. While the data generated at 0.5 m per second, using the upgraded servo-hydraulic system is useful to the pipeline designers, we also need data generated at crack velocities approaching those of real events (more than 100 m per second). To that end, we have constructed a spring fixture that is expected to produce crack velocities exceeding 300 m/s in our MDCB specimens. The fixture parts were ordered and have been assembled (Figure 6) and will be installed in the test machine in the next quarter to generate true dynamic rate CTOA tests. Currently, we are machining CTOA test specimens to generate CTOA data at the high-speed rate. We plan to test at 2 rates: the first using the modified servo-hydraulic machine rate, and the second using the spring fixture. We expect this data to be available for the next quarterly report.



**Figure 6.** Spring apparatus for dynamic CTOA testing.

**Dynamic Kolsky Bar Testing:** The high strain rate plastic flow properties of high strength pipeline steels at sub-ambient temperatures will be examined at NIST Gaithersburg using a temperature controlled Split-Hopkinson Pressure Bar (Kolsky Bar) apparatus. For a running ductile fracture in a gas pipeline, the ability of a steel to strengthen near the crack tip, where the strain rate is very high, has an important impact on the propagation and arrest behavior of the fracture. Strain rate effects on the strengthening of different grades of pipeline steel have already been investigated at ambient temperature using the Kolsky Bar. We will now extend the study to examine how temperature influences the strengthening behavior of these steels with increasing strain rate. Decreasing temperatures tend to increase the strength of steel, much like increasing strain rates. As a result, the capacity of steel to strengthen may decrease with temperature, meaning ductile fractures may propagate more easily in pipelines that are buried in cold environments. Kolsky Bar measurements of pipeline steels will be used to help discriminate the strain rate strengthening capacity of available pipeline steel materials at cold temperatures, so that optimal fracture-resistant steels can be chosen for high pressure gas pipelines.

During this quarter, modifications to the existing Kolsky Bar were made to test samples at sub-ambient temperatures, including the addition of helium cooling jets and a thermocouple for monitoring and controlling the sample temperature prior to the test. Our plans are to test pipeline steel samples at temperatures between ambient and -80 °C to determine how their high strain rate response varies with service temperature. This data will aid in the estimation of the fracture-resistance of pipeline steels.

**Single Edge Notch Tension Testing:** Work is progressing on the test development for the single edge notch tensile [SEN(T)] test. This test technique was specifically developed in response to technological advances in the oil and gas pipeline industry. Fracture toughness values (K, CTOD, J and J-resistance) have, in the past, been derived through bend testing. These values are used to determine critical flaw sizes for the determination of various levels of an engineering critical assessment (ECA). Bend testing has historically been used to determine these values. However, in many cases, values determined through bend testing provide an overly conservative result and is not representative of real pipeline operational conditions. Pipeline service conditions are typically better represented in a tensile mode. Therefore, we have chosen to better represent the lower constraint conditions of the in-service pipeline through the single edge notch tensile test (SEN(T)).

This fracture toughness test will be used to determine the ductile-to-brittle transition temperature for the X100 pipeline steel; we will be testing at temperatures from room temperature down to -80°C. Protocols similar to those used at SINTEF Materials Technology will be employed. The low temperature test chamber has been set up and tested for temperature variation. Test fixturing has been designed and materials have been acquired and are currently in the machine shop for machining. Specimens are also being machined to test our methods and protocols. The actual testing will begin early in the next quarter.

## **Modeling:**

**The GTN Damage Model:** Modeling of ductile failure is often carried out with the model by Gurson, Tvergaard and Needleman (GTN). Münstermann et al. [1] provides an excellent summary of the GTN model developed back in the 80's. The core of this model is a yield potential considering the effect of microstructural damage on the yielding behavior. This yield potential was developed for a spherical body made of a ductile matrix material containing a spherical void [2-6].

Altogether, nine parameters of the GTN model have to be quantified for damage modeling:  $q_1, q_2, q_3, f_0, f_N, \epsilon_N, S_N, f_c$  and  $f_f$ .

With:

$q_1, q_2, q_3$ : model parameters,  
 $f_0$ : initial void volume fraction,  
 $f_N$ : nucleation of the volume fraction,

- $\varepsilon_N$  :            equivalent plastic strain,
- $S_N$  :            specific standard deviation,
- $f_c$  :            critical void volume fraction,
- $f_f$  :            void volume fraction at macroscopic failure.

In the following paragraphs, guidelines for quantification of these model parameters are given.

The evolution of ductile damage in steel can be divided into three phases, as seen in Figure 7: void nucleation, void growth and void coalescence. Three mechanisms combine in the last phase, as seen in Figure 8: growing together of voids, ligament necking and nucleation of secondary voids.

**Initial porosity.** As nucleation of primary voids is considered to take place at the onset of plastic deformation, the amount of primary void initiating constituents can be understood as initial porosity  $f_0$ . For many steel grades, non metallic inclusions are reported to be responsible for primary void nucleation [6], but it can also be caused by martensitic phases in multiphase steels or other hard microstructure constituents of sufficient size. Quantification of primary void nucleating microstructural constituents is often carried out by means of scanning electron microscopy (SEM) and x-ray spectroscopy (EDX): Polished surfaces are scanned, and an automatic image analysis is employed to differ between matrix material and second phases. After determination of the second phase's chemical composition by EDX analysis, a differentiation of the void nucleating constituents can be carried out. Results from the image analysis provide size and shape of each detected second phase, so that the initial porosity  $f_0$  can be calculated.

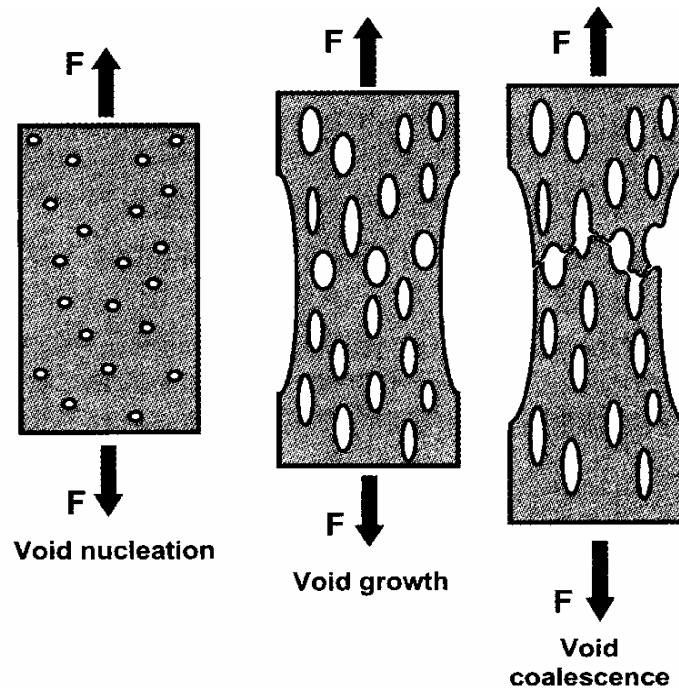


**Figure 7.** Schematic representation of the ductile damage development in metals.

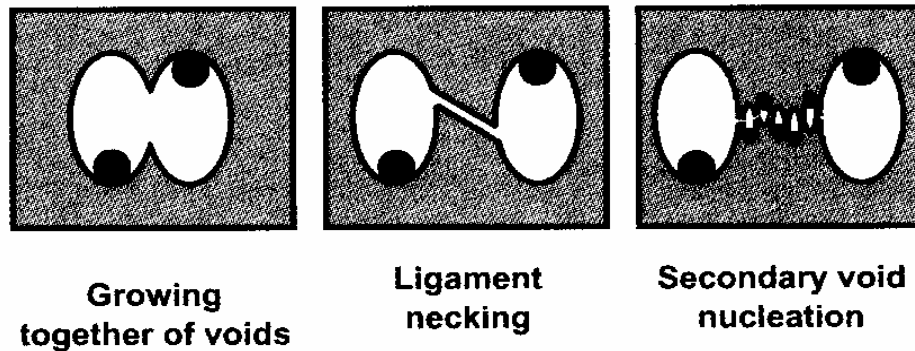


**Figure 8.** Mechanisms of void coalescence.

**Volume fraction of secondary voids.** Secondary voids are assumed to nucleate during primary void coalescence at smaller microstructural constituents like precipitations or, in case of multiphase steels, small carbon-enriched zones like fine-dispersed bainitic islands [7]. It can be concluded that the amount of secondary void nucleating microstructure constituents can be understood as the volume fraction of newly-nucleating voids  $f_N$  and that a procedure for their quantification corresponds to the determination of primary void nucleating sites. Nevertheless, in many cases problems are encountered during experimental quantification of the secondary void nucleating sites due to their small size. Thus, the parameter  $f_N$  is often fit to achieve good agreement between experiments and simulations.

**Characteristic strain of secondary void nucleation.** Quantification of the characteristic strain  $\varepsilon_N$  of secondary void nucleation can be carried out by using notched tensile tests. After identification of the characteristic load leading to void nucleation, the strain  $\varepsilon_N$  can be calculated numerically by FEM [1].

**Standard deviation of strain controlled secondary void nucleation.** The standard deviation  $S_N$  : of the strain- controlled nucleation of secondary voids is usually not subject to parameter studies. Instead,  $S_N = 0.1$  is commonly used [8]. Reasons for this selection are, on the one hand, that the parameter  $S_N$  is reported to have a negligible influence on simulation results and, on the other hand, that the model of strain-controlled nucleation of secondary voids is a rough interpretation of ductile damage evolution in steels.

**Critical void volume fraction.** Different methods are available for quantification of the critical void volume fraction  $f_c$ . One possibility is to carry out cell model simulations for modeling the behavior of a void in a matrix material which is externally stressed, such as in a notched tensile test. In such simulations, the critical void volume fraction  $f_c$  leading to accelerated void growth can be determined.

**Final void volume fraction.** Concerning the void evolution law, the last parameter to be quantified is the final void volume fraction  $f_f$ . In the past, density measurements were carried out for its determination. These had to be quite accurate due to the low  $f_f$  values which are in a range of only 10% to 20% for many steels. Figure 9 shows final voids, after failure of an X100 tensile test.

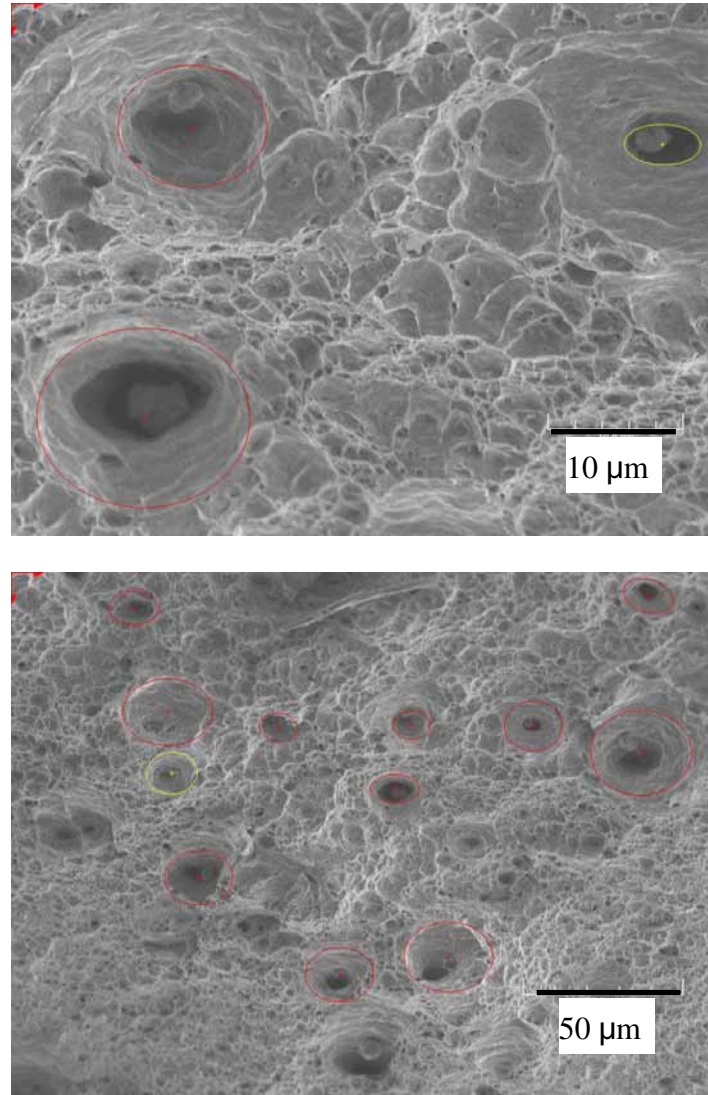


**Figure 9.** Final voids on X100 tensile fracture surface test.

**GTN yield potential parameters.** The model parameters  $q_1, q_2$  and  $q_3$  can either be selected due to the recommendations by Tvergaard and Needleman, or they can be determined numerically in cell model calculations. Therefore, single (or multi) voided cells are loaded numerically under constant external triaxiality and the homogenized stresses and strains are used as a reference for GTN calculations with varying parameters

[1]. The calculations show that the  $q$ -parameters depend slightly on triaxiality, and that the estimation of constant values is generally acceptable [9].

**Simulation.** The GTN model has been used for FE simulation in the commercial finite element code ABAQUS/Explicit 6.6. The fracture behavior of the MDCB (Modified Double Cantilever Beam) CTOA (Crack Tip Opening Angle) test is being investigated in 2D and 3D. Figure 10 presents the 2D and 3D FE models.

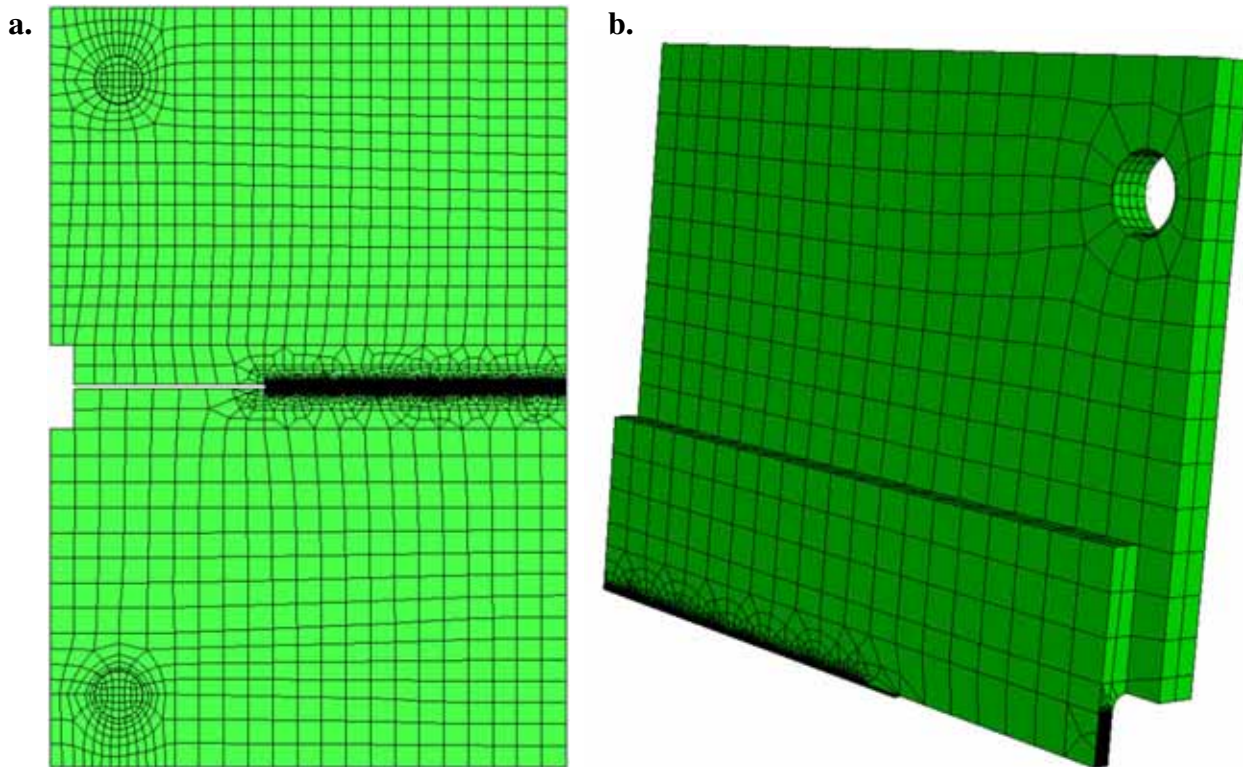


**Figure 10.** a. 2D Finite Element model, b. 3D Finite Element model.

The GTN parameters are currently being calibrated by using a parametric study of the models, which is, computationally, very time consuming. We expect to have results soon.

- [1] S. Münstermann, U. Prahl, W. Bleck: *Numerical modeling of toughness and failure processes in steel structures*, Steel Research Int., 78 (2007), No. 3, 224-235.
- [2] A.L. Gurson: J. Engn. Mater. Tech., 99 (1977), 2.
- [3] V. Tvergaard: *On localization in ductile material containing spherical voids*, Int. J. Fract., 18 (1982), 237-252.
- [4] V. Tvergaard, A. Needleman: *Analysis of the cup-cone fracture in a round tensile bar*, Acta. metall., 32 (1984), No.1, 157-169.
- [5] A. Needleman, V. Tvergaard: *An analysis of ductile rupture modes at a crack tip*, J. Mech. Phyc. Solids., 35 (1987), 151-183.
- [6] V. Tvergaard. A. Needleman: *Effect of Crack Meandering on Dynamic, Ductile Fracture*, J. Mech. Phys. Solids., 40 (1992), No. 2, 447-471.

- [7] W.M. Jr. Garrison, N.R. Moody: *Ductile fracture*, J. Phys. Chem. Solids., 48 (1987),No. 11, 1035-1074.
- [8] M. Springmann, M. Kuna: *Identification of material parameters of the Gurson–Tvergaard–Needleman model by combined experimental and numerical techniques*, Comp. Mat. Sci., 32 (2005), 501-509.
- [9] G. Bernauer, W. Brocks: *Micro-mechanical modelling of ductile damage and tearing – results of a European numerical round robin*, Fatigue Fract. Engng. Mater. Struct., 25 (2002), 363-384.

## Task 4: CTOA Fracture Surface Evaluation

**Fracture Surface Evaluations:** The fracture surface features (and microstructure) of CTOA and tensile specimens are being characterized for input to models of pipeline failure. For example, the most dominant features on the slant surface of the 35 ksi yield strength pipeline steel shown in Figure 11 are shallow ductile dimples, on the order of 10 micrometers in diameter. These larger, shallow dimples typically contain many smaller ductile dimples within them. In comparison, the characteristic features found on the slant fracture regions of X65 specimens (Figure 12), are considerably less textured. The fracture surface in the shear region of this X65 CTOA sample has very shallow ductile dimples, and a significantly smoother texture than the fracture surface shown in Figure 7. This difference is assumed to be due to differences in the microstructure and strength of the steels, and we are gathering data to help quantify the variables. Our initial findings indicate that the texture associated with the shear regions on X65 CTOA samples becomes smoother as the velocity of the crack growth increases. Our plan is to characterize the features for X65 and X100 steels for a range in crack velocities that covers several orders of magnitudes. The velocity ranges and test methods are described in the Dynamic CTOA section of the report.

The plastic flow associated with the fracture of CTOA specimens (Figures 11 and 12) results in significant thinning in the cross section of the sample. In the case of the quasi-static tested X100 sample plotted in Figure 13, thinning occurred over for a distance of about 5 times the thickness. The profile and magnitude of this thinning can be compared with measurements for the X100 full scale rupture test (dynamic fracture), shown in Figure 14, which shows thinning occurred at a distance of about

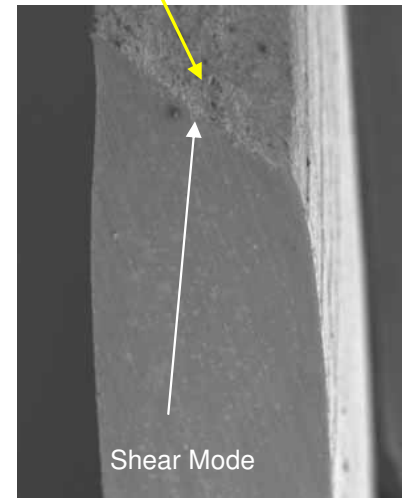
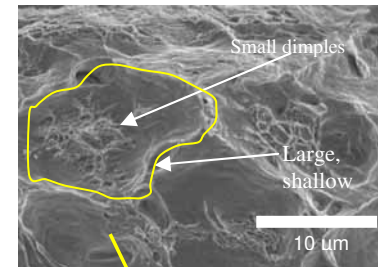


Figure 11: Cross section through CTOA sample showing plastic deformation and slant fracture: 3 mm thick, 35 ksi, ferrite-pearlite pipeline steel)

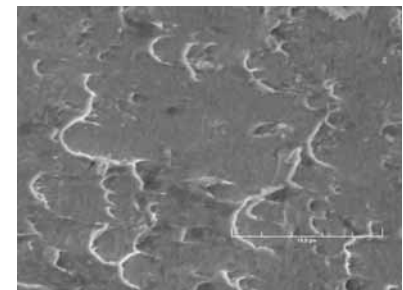


Figure 12: Slant (shear lip) fracture region on 8mm X65.

10 times the thickness of the pipe wall. Note that our CTOA sample design (modified double cantilever beam (MDCB)) has an increase in thickness (shoulder) that restricts the plastic flow. Dynamic CTOA tests have not yet been conducted for the X100 steel, but, if results for the X65 steel are any indication, the plastic flow for the quasi-static and dynamic CTOA tests will not differ significantly.

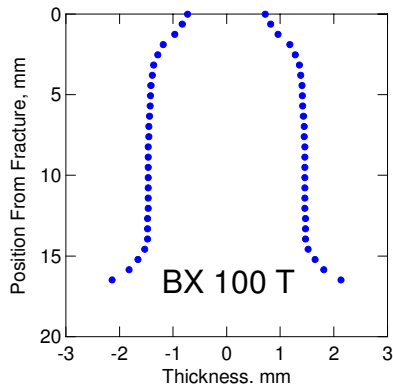


Figure 13: Profile of thinning for a CTOA sample of X100 steel

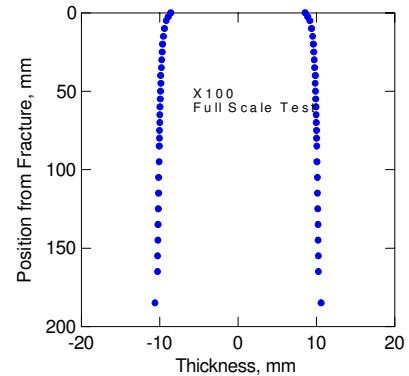


Figure 14: Profile of thinning for the X100 full scale burst test.

## Task 5: Method for determination of yield strength in high strength pipeline steels and welds

To better understand the role of yield to tensile ratio (Y/T) in high strength pipeline steels, we plan to review the stress-strain curves generated on the pipeline steels used throughout this research program. The yield strengths vary from about 30 ksi to about 100 ksi. The lower strength steels typically have a low Y/T and the higher strength steels have a high Y/T. All specimens used in our study have been machined directly from the pipeline wall and were not flattened so as to minimize the Bauschinger effect, providing an unaltered deformation history (timeline starting at pipeline fabrication completion). Pipeline specimens were machined into round specimens when possible and flats when necessary because of small wall thickness. The high strength (X100) pipeline specimens were always machined into round specimens.

Flattening of the pipeline wall material prior to specimen machining introduces stresses that alter the yield strength values. Current API practice requires that specimens be flattened prior to testing. This flattening requirement coupled with the high-strength steel high Y/T creates a dilemma for pipeline designers today. A better understanding of yield strength determination in high-strength pipeline steels would benefit pipeline designers for their strain-based design requirements.

## **Task 6: Other tasks**

In addition to supporting this effort through laboratory research, NIST representatives have attended PSIA meetings, reviewed proposals and peer-reviewed projects as needed. A presentation was given on our CTOA efforts to ASTM Committee E08 on Fracture Mechanics. Reports published or submitted for publication, conferences attended and symposia participation during this quarter are as follows:

### Papers

#### **Measurement of Weld Toughness - Crack Tip Opening Angle Criterion -**

Ph. P. Darcis, J. D. McColskey, C. N. McCowan and Tom Siewert  
Welding Journal, June, 2007.

#### **Crack Tip Opening Angle Optical Measurement Methods in Five Pipeline Steels**

Ph. P. Darcis, C. N. McCowan, H. Windhoff, J. D. McColskey and T. A. Siewert  
Engineering Fracture Mechanics, *to be published (submitted in February 2007)*.

### Conferences

#### **Fracture Toughness through a Welded Pipeline Section - Crack Tip Opening Angle Criterion -**

Ph. P. Darcis, C. N. McCowan, E. S. Drexler, J. D. McColskey, A. Shtechman and T. A. Siewert, International IIW conference Welding & Materials Technical, economic and ecological aspects, Cavtat & Dubrovnik, Croatia, July 05-06, 2007.

### ASTM presentation

#### **Crack Tip Opening Angle Measurement: Pipeline Steels**

C. N. McCowan, Ph. P. Darcis, J. D. McColskey, A. Shtechman, T. A. Siewert, J. M. Treinenand and H. Windhoff  
ASTM International, E 2472-06 Standards Meeting, Norfolk, VA, USA, May 21-23, 2007.

### NIST-CU Symposium

#### **Fracture toughness of high strength pipeline steels - CTOA criterion**

Ph. P. Darcis, G. Kohn, A. Bussiba, J. D. McColskey, C. N. McCowan, T. A. Siewert, J. Merritt, R. Smith and N. Sanderson  
2nd Annual University of Colorado, Boulder and National Institute of Standards and Technology (NIST) Research Symposium, Boulder, Colorado, USA, March 22, 2007.

#### **Fatigue Properties of Aged and New Pipeline Steels**

Ph. P. Darcis, G. Kohn, A. Bussiba, J. D. McColskey, C. N. McCowan, T. A. Siewert, J. Merritt, R. Smith and N. Sanderson

2nd Annual University of Colorado, Boulder and National Institute of Standards and Technology (NIST) Research Symposium, Boulder, Colorado, USA, March 22, 2007.

**Pipelines for the hydrogen economy**

J. D. McColskey, Ph. P. Darcis and T. A. Siewert

2nd Annual University of Colorado, Boulder and National Institute of Standards and Technology (NIST) Research Symposium, Boulder, Colorado, USA, March 22, 2007.

**Reporting**

This is the fourth quarterly report under agreement number DTPH56-06-X-000029. The next quarterly report will be submitted in 3 months.